doi: 10.15407/ujpe60.09.0925

V.V. STRELCHUK,[1] A.S. NIKOLENKO,[1] YU.YU. STUBROV,[1] A.E. BELYAEV,[1] V.O. GUBANOV,[2] M.M. BILIY,[2] L.A. BULAVIN[2]

[1] V.E. Lashkaryov Institute of Semiconductor Physics, Nat. Acad. of Sci. of Ukraine
(45, Nauky Pr., Kyiv 03028, Ukraine; e-mail: chig-ua@rambler.ru)
[2] Faculty of Physics, Taras Shevchenko National University of Kyiv
(64, Volodymyrs'ka Str., Kyiv 01601, Ukraine)

PHONON ENERGY SPECTRA AND STATIONARY ELASTIC WAVES IN SINGLE-WALLED CARBON NANOTUBES AND GRAPHITE BULK CRYSTALS

PACS 63.22.-m

Micro-Raman spectra of single-walled carbon nanotubes, graphite bulk crystals, one-layer and two-layer graphenes are investigated in detail. The structure of Davydov multiplets in the energy spectra of electronic states of one-layer and two-layer graphenes and Bernal graphite bulk crystals is established. The energy spectra of vibrational and electronic states of nanotubes and graphite bulk crystals are shown to be described by the dispersion curves, which pairwise joint at points A of the Brillouin zones of these structures. The forms of stationary elastic waves in single-walled carbon nanotubes at Γ *and A points of their Brillouin zones and in one-layer and two-layer graphenes and bulk graphite at* Γ*, K, and M points of their Brillouin zones are analytically calculated.*

K e y w o r d s: micro-Raman spectroscopy, arc-discharge method, stationary elastic waves, double Davydov splitting, macromolecular class.

1. Introduction

The discovery of a two-dimensional monolayer of carbon atoms (graphene) in 2004 [1], which is the building block for various forms of graphite materials, has risen a growing interest in investigations of the properties of all kinds of these structures and, particularly, of single-walled carbon nanotubes, n-layer graphenes, and graphite bulk crystals. This interest is mainly caused by unusual electronic properties of one-layer graphene, which arise from the linear dispersion of valence and conduction band electronic states touching each other at the K-point of the two-dimensional Brillouin zone. Such behavior of the electron dispersion allows detailed investigations of electron-phonon resonances in the optical range of excitations [2].

A unit cell of the honeycomb lattice of one-layer graphene contains two crystallographically unequivalent atoms of carbon. Two π-orbitals of carbon atoms of a single unit cell form dispersive bonding and antibonding orbital states, which correspond to valence and conduction bands. These states for each wave vector $\mathbf{k}$ of the one-layer graphene Brillouin zone are the components of doublets caused by the Davydov splitting (DS) of electron π-zones.

A single graphene layer is known to be a semimetal (or zero-gap semiconductor) with a linear Dirac-like spectrum around the Fermi energy, while n-layer graphenes ($n \geq 2$) and graphite bulk crystals have parabolic electron spectra revealing the semimetallic behavior with a band overlap increasing with n for n-layer graphenes from 0.16 meV ($n = 2$) to 41 meV for graphite bulk crystals [3].

Micro-Raman spectroscopy is a powerful tool for investigations of electron and phonon excitations and defects in microstructure carbon-based materials [4], [5]. The existence of the double electron-phonon resonance mechanism (DR) enables effective studies of second-order phonon processes in n-layer graphenes, bulk graphite crystals, and single-walled carbon nanotubes (SWCNTs) [6].

In the present paper, the structure of Davydov multiplets in the electron and phonon spectra of n-layer graphenes, graphite bulk crystals, and SWCNTs is investigated experimentally, by using the micro-Raman

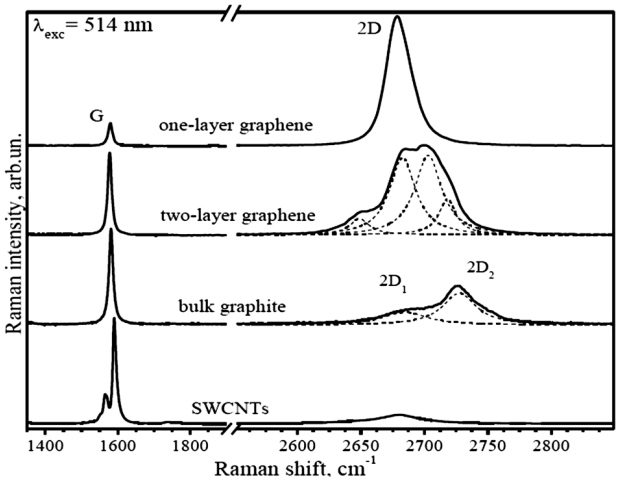

Fig. 1. Raman spectra of single-layer graphene, two-layer graphene, bulk graphite, and single-walled carbon nanotubes measured at room temperature; the excitation wavelength $\lambda_{\rm exc} = 514.5$ nm

technique and theoretically using projective representations of symmetry group theory. Dispersion behavior of vibrational excitations in Γ-A directions of the Brillouin zones of graphite bulk crystal and SWCNTs is established. Forms of normal vibrations for phonons and stationary elastic waves at $\mathbf{k} \neq 0$ points of the Brillouin zones of these structures are also calculated.

2. Experimental

Investigated micrometer-scaled single and multilayer graphene sheets were prepared by the mechanical exfoliation of highly oriented pyrolytic graphite. The layers were deposited onto Si substrates covered with a 300-nm-thick layer of thermal SiO_2 used for the visual observation of graphene by means of optical microscopy [7]. The thickness of n-layer graphene samples was confirmed by the analysis of 2D Raman modes [8].

Single-walled carbon nanotubes used in this study were synthesized by the arc-discharge method in a 600-mbar He atmosphere with nickel and yttrium oxides as catalysts. The diameter distribution of the investigated carbon nanotubes mixture was estimated from the experimental frequencies of radial breathing modes (RBM) as $d_t = 1.51 \pm 0.30$ nm [9].

Micro-Raman spectra were measured in the backscattering geometry at room temperature, by using a triple Raman spectrometer T-64000 Horiba Jobin–Yvon equipped with a cooled CCD detector. The line of an Ar–Kr ion laser with a wavelength of 514.5 nm was used for the excitation. Excited radiation was focused on the sample surface with a 50x optical objective. The laser power on the sample surface was always kept below 1 mW, in order to obtain the acceptable signal-to-noise ratio and to prevent the laser heating effect.

3. Results and Discussion

Figure 1 shows the Raman spectra of one-layer graphene, two-layer graphene, monocrystalline Bernal graphite with $(ab)_n$-stacking, and single-walled carbon nanotubes (SWCNTs). It can be seen that the micro-Raman spectra of one-layer graphene contain the intense single 2D-line, besides the G-band allowed in the first-order scattering processes caused by twofold degenerated valence intra-layer vibrations of C-atoms. This band is due to second-order processes for phonons at K-point. The intensity of the 2D-band approximately five times larger than the G-band intensity, i.e. $I_{\rm 2D}/I_{\rm G} \approx 5$. Micro-Raman spectra of two-layer graphene, besides the G-band, also contains the 2D-band, but consisting of four components. As can be seen from Fig. 1, the 2D-band is well approximated by four Lorentz contours. The 2D-band in the Raman spectrum of monocrystalline graphite contains only two components, reflecting the structure of electronic bands of 3D Bernal graphite. The G-band of SWCNTs Raman spectrum consists of two components G_1 (1565.6 $\rm cm^{-1}$) and G_2 (1590.5 $\rm cm^{-1}$), which are the components of a chiral doublet. The G_2-band corresponds to valence vibrations of armchair nanotubes perpendicular to the nanotube axis, and the G_1-band – to valence vibrations of zigzag nanotubes parallel to the nanotube axis. The 2D line at 2680.4 $\rm cm^{-1}$ in this spectrum contains only one component.

Figure 2 shows the results of calculations of the valence (π) and conduction (π^*) bands of one- and two-layer graphenes [10] and bulk graphite crystal [11]. For each value of wave vector $\mathbf{k}$ of the one-layer graphene Brillouin zone, these bands are the components of a Davydov doublet arising from DS of electronic states, which correspond to symmetric (bonding) and anti-symmetric (anti-bonding) linear combinations of atomic π-orbitals: for the valence band, $\psi_c = (1/\sqrt{2})(\varphi_1 + \varphi_2)$ and, for the conduc-

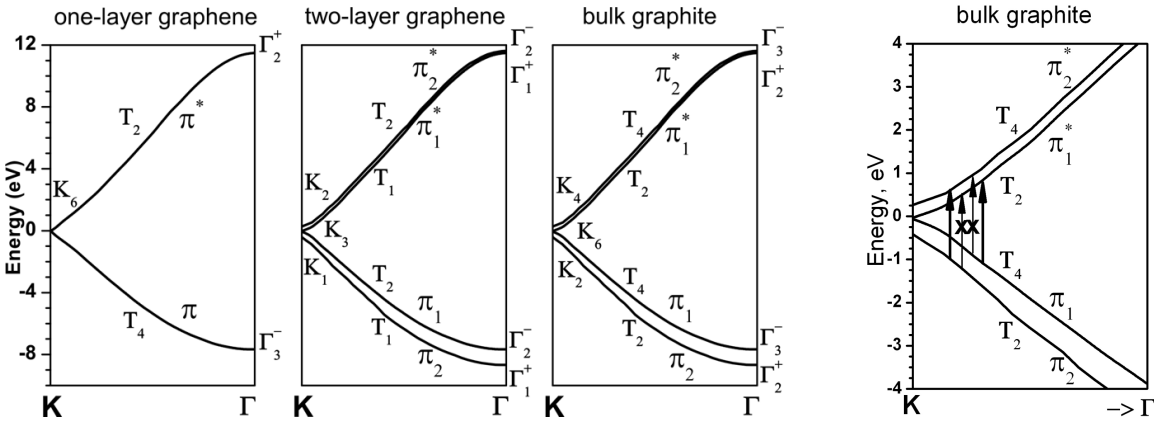

Fig. 2. Schematic electronic dispersion for π-electrons and the irreducible representations for one-layer graphene [10], two-layer graphene [10], and bulk graphite crystal [11]

Fig. 3. Scheme of allowed and forbidden electronic transitions in a bulk graphite crystal

tion band, $\psi_c = (1/\sqrt{2})(\varphi_1 - \varphi_2)$, where indices 1 and 2 correspond to the π-orbitals of the first and second carbon atoms belonging to a single unit cell. Symmetry of π-zones is indicated in notation of irreducible representations according to [12]. At K points (Dirac points), the π and π^* zones touch each other, and their symmetry at these points is described by the two-dimensional irreducible representation K_6 (K_3^- in notation [10]) of the wave vector group, which is isomorphic to the point group D_{3h}.

As was mentioned above, the 2D line in the Raman spectra of two-layer graphene consists of four components. The interlayer interaction in two-layer graphene leads to an increase of the number of 2D line components as compared with one-layer graphene, which connects with DS of electronic states of one-layer graphene. The rather weak interlayer interaction leads to small DS of π-zones of one-layer graphene, which could be called the double Davydov splitting (DDS) in two-layer graphene. The dispersion of electronic states near the K-point in such graphene has parabolic behavior instead of a linear behavior of one-layer graphene [3].

The structure of electronic π-zones at Γ-point of 3D graphite (Fig. 2) is determined by irreducible representations of the 6/mmm (D_{6h}) symmetry group:

$$\Gamma_\pi = \Gamma_{\text{eq}} \otimes \Gamma_z = 2\Gamma_2^+ + 2\Gamma_3^-,$$

where Γ_{eq} and Γ_z are the equivalent and π-orbital representations of the 6/mmm group.

The group of the wave vector at K-point of Bernal graphite Brillouin zone is isomorphic to the $\overline{6}m2(D_{3h})$ point group. The structure of π-zones at K-point (Fig. 2) is determined by the irreducible representation of the $\overline{6}m2$ group:

$$K_\pi = K_{\text{eq}} \otimes K_z = K_2 + K_4 + K_6.$$

In view of the anisotropy of optical absorption (emission), the electronic transition matrix element should be proportional to $|\mathbf{P} \times \mathbf{k}|^2$ [13], where $\mathbf{P}$ is the polarization of incident (scattered) light in absorption (emission) processes, and $\mathbf{k}$ is the electron wave vector measured from K-point. In this case, only electronic transitions $\pi_1 \rightleftharpoons \pi_1^*$ and $\pi_2 \rightleftharpoons \pi_2^*$ are allowed, and the transitions $\pi_2 \rightleftharpoons \pi_1^*$ and $\pi_1 \rightleftharpoons \pi_2^*$ become forbidden, as is shown in Fig. 3.

In bilayer graphene, the anisotropy of optical transitions is less sufficient than for bulk crystalline graphite, and the transitions $\pi_2 \rightleftharpoons \pi_1^*$ and $\pi_1 \rightleftharpoons \pi_2^*$ become also allowed. It is also clear from the scheme shown in Fig. 3 that, as a result of the $\pi_1 \rightleftharpoons \pi_1^*$ transitions, an electron obtains the momentum almost two times bigger than in case of $\pi_2 \rightleftharpoons \pi_2^*$ transitions. This means that, in DR processes with the electronic transition $\pi_1 \rightleftharpoons \pi_1^*$, the energy of iTO phonons taking part in such processes considerably exceeds the energy of iTO phonons in DR processes with $\pi_2 \rightleftharpoons \pi_2^*$ electronic transitions.

Thus, the $2D_2$ component in the Raman spectra of bulk graphite (Fig. 1) at 2727.5 cm^{-1} (iTO phonon wave number of 1363.8 cm^{-1}) corresponds to the electronic transition $\pi_1 \rightleftharpoons \pi_1^*$, and the component $2D_1$ at 2684.9 cm^{-1} iTO phonon wave number of 1342.5 cm^{-1}) – $\pi_2 \rightleftharpoons \pi_2^*$ electronic transition.

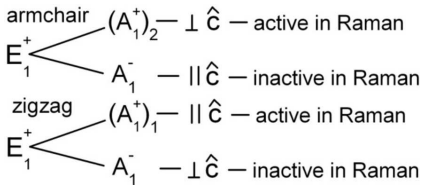

Fig. 4. Scheme of splitting of graphene double degenerated vibrations of E_1^+ symmetry in armchair and zigzag SWCNTs. The signs ⊥ and ∥ denote perpendicular and parallel directions of atom displacements relative to the SWCNT axis

In Fig. 4, the scheme of graphene valence vibration splitting and the process of formation of the doublets caused by chiral anisotropy in carbon nanotubes of different chiralities are demonstrated.

Carbon single-walled nanotubes of infinite lengths have been considered as crystals with periodicity along one direction, i.e. crystals possessing the one-dimensional translation symmetry. Such symmetry leads to the appearance of symmetry elements such as screw axes and sliding reflection plains [14, 15], the same as in the case of two- and three-dimensional periodicities [16, 17]. Nanotubes and two-periodic graphene sheets can be considered as macromolecules or one- and two-periodic crystals. We will describe the symmetry of one-periodic structures using one-periodic space groups (OnG), which are the groups of cylindric symmetry (CSG). So the symmetries of armchair and zigzag SWCNTs with chiral indices (n, n) and $(n, 0)$, respectively, will be described by one-periodic space groups in Schoenflies notations, as OnG (or CSG) $D_{2nh} - 1$, which contain neutral screw axes $(2n)_n$ and n sliding reflection plains. Arabic numerals 1, 2, 3,... of these notations point out the sets of nontrivial translations, which are realized in such nonsymmorphic or symmorphic classes of the space symmetry group. Set 1 of the basic elements h_i, for example, for armchair (3, 3) and zigzag (3, 0) SWCNTs, which is determined by the space group CSG $D_{6h} - 1$ and, for Bernal crystalline graphite with space symmetry group $P6_3/mmc(D_{6h}^4)$, may be chosen, as it is shown in relation (1), where $\mathbf{a}$ — the basic lattice vector along the c_6-axis – coincides with the OZ (Oz) direction.

The symmetry of physical properties of such one- or two-periodic structures, including the energy spectra of vibrational and electronic states, is described by all the nanotube and graphene sheet inequivalent directions. Such point symmetry group for one- and two-periodic structures could be called the "macromolecular class" group. The term "macromolecular class" for one- and two-periodic structures is an analog of the "crystalline class" for three-periodic structures. We have

$$\begin{cases} h_1 = (0|e), \quad h_2 = (0|c_3), \quad h_3 = (0|c_3^2), \\ h_4 = (0|(u_2)_1),\ h_5 = (0|(u_2)_2),\ h_6 = (0|(u_2)_3), \\ h_7 = \left(\frac{\mathbf{a}}{2}\middle| c_2\right),\ h_8 = \left(\frac{\mathbf{a}}{2}\middle| c_6^5\right),\ h_9 = \left(\frac{\mathbf{a}}{2}\middle| c_6\right), \\ h_{10} = \left(\frac{\mathbf{a}}{2}\middle| (u_2^{'})_1\right),\ h_{11} = \left(\frac{\mathbf{a}}{2}\middle| (u_2^{'})_2\right), \\ h_{12} = \left(\frac{\mathbf{a}}{2}\middle| (u_2^{'})_3\right),\ h_{13} = (0|i),\ h_{14} = (0|ic_3), \\ h_{15} = (0|ic_3^2), h_{16} = (0|(\sigma_d)_1), h_{17} = (0|(\sigma_d)_2), \\ h_{18} = (0|(\sigma_d)_3), h_{19} = \left(\frac{\mathbf{a}}{2}\middle| \sigma_k\right), h_{20} = \left(\frac{\mathbf{a}}{2}\middle| ic_6^5\right), \\ h_{21} = \left(\frac{\mathbf{a}}{2}\middle| ic_6\right),\ h_{22} = \left(\frac{\mathbf{a}}{2}\middle| (\sigma_d^{'})_1\right), \\ h_{23} = \left(\frac{\mathbf{a}}{2}\middle| (\sigma_d^{'})_2\right),\ h_{24} = \left(\frac{\mathbf{a}}{2}\middle| (\sigma_d^{'})_3\right). \end{cases} \quad (1)$$

To study the dispersion of elementary excitations, we constructed the irreducible projective representations of wave vector groups at various Brillouin zone points of carbon nanotubes, graphene sheets, and graphite crystals. In order to find these representations, we have calculated the factor-systems, according to the following formulae [12]:

• for one-valued representations (for integer spin),

$$\omega_{1,\mathbf{k}}(r_2, r_1) = e^{i(\mathbf{k} - r_2^{-1}\mathbf{k})\boldsymbol{\alpha}_1}, \quad (2)$$

which is determined by the space group properties, $\boldsymbol{\alpha}_1$ – the vector of nontrivial translation of h_i element),

• and the two-valued representations (for half-integer spin)

$$\omega_2(r_2, r_1) = \begin{cases} 1 & \text{at} \quad 0 \le \vartheta < 2\pi, \\ -1 & \text{at} \quad 2\pi \le \vartheta < 4\pi, \end{cases} \quad (3)$$

which describes the transformations of spin functions (ϑ is the rotation angle corresponding to $r_2 r_1$ element).

In [18], the classification of projective classes of the point group $6/mmm(D_{6h})$ is presented. The group $6/mmm$ has 8 classes of projective representations, which are classified, by using the system of three coefficients α, β, and γ with the values 1 or —1. Each of

Table 1. **The characters of one- and two-valued projective representations for A-points for armchair and zigzag carbon nanotubes and bulk graphite crystals**

Class	Notation of irreducible projective representation	e	c_3	c_3^2	$3u_2$	c_2	c_6^5	c_6	$3u_2'$	i	ic_3	ic_3^2	$3\sigma_d$	σ_h	ic_6^5	ic_6	$3\sigma_d'$
K_5	A_1	2	2	2	0	0	0	0	0	0	0	0	2	0	0	0	0
	A_2	2	2	2	0	0	0	0	0	0	0	0	−2	0	0	0	0
	A_3	4	−2	−2	0	0	0	0	0	0	0	0	0	0	0	0	0
K_4	A_4	2	−2	2	2i	0	0	0	0	0	0	0	0	0	0	0	0
	$A_4 + A_5 \langle$																
	A_5	2	−2	2	−2i	0	0	0	0	0	0	0	0	0	0	0	0
	A_6	4	2	−2	0	0	0	0	0	0	0	0	0	0	0	0	0

them is determined by $[\omega(r_j, r_i)]^{-1}\omega(r_i, r_j) = \frac{\omega(r_i, r_j)}{\omega(r_j, r_i)}$ ratio for the corresponding pair of commutating elements r_i and r_j from generating elements or elements of classes, which contain generating elements. As such generating elements for the group, we can choose, for example, the following elements:

$$a = r_1 = (u_2)_1, \quad b = r_2 = c_2 \quad \text{and} \quad c = r_3 = i.$$

In our case,

$$\alpha = \frac{\omega(a,b)}{\omega(b,a)} = \frac{\omega[(u_2)_1, c_2]}{\omega[c_2, (u_2)_1]},$$
$$\beta = \frac{\omega(a,c)}{\omega(c,a)} = \frac{\omega[(u_2)_1, i]}{\omega[i, (u_2)_1]},$$
$$\gamma = \frac{\omega(b,c)}{\omega(c,b)} = \frac{\omega[c_2, i]}{\omega[i, c_2]}.$$

For the classification and the notation of factor-system classes and the corresponding projective representation classes in the 6/mmm group, it is convenient to choose the following system of classes, which differs from the presented in [12]:

$K_0 - \alpha = 1, \quad \beta = 1, \quad \gamma = 1;$

$K_1 - \alpha = -1, \quad \beta = 1, \quad \gamma = 1;$

$K_2 - \alpha = 1, \quad \beta = -1, \quad \gamma = 1;$

$K_3 - \alpha = -1, \quad \beta = -1, \quad \gamma = 1;$

$K_4 - \alpha = 1, \quad \beta = 1, \quad \gamma = -1;$

$K_5 - \alpha = -1, \quad \beta = 1, \quad \gamma = -1;$

$K_6 - \alpha = 1, \quad \beta = -1, \quad \gamma = -1;$

$K_7 - \alpha = -1, \quad \beta = -1, \quad \gamma = -1.$

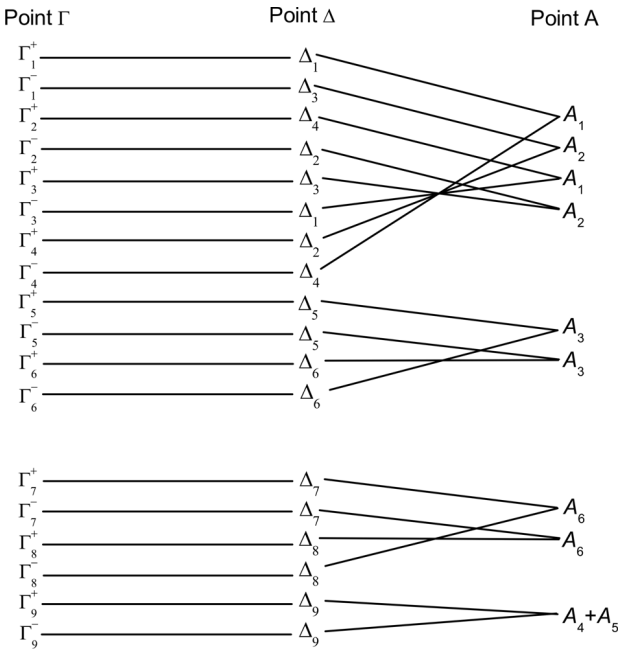

Fig. 5. Diagram determining the compatibility relations of irreducible projective representations along Γ–A lines in the Brillouin zones of three-periodic bulk graphite crystals and one-periodic SWCNTs

For A-points of the Brillouin zones of carbon nanotubes and graphite crystals, we constructed, by using relation (1) and formulae (2) and (3), the factor-systems $\omega_{1,A}(r_2, r_1)$ and $\omega_{2,A}(r_2, r_1) = \omega_{1,A}(r_2, r_1) \times \times \omega_2(r_2, r_1)$, found the values of α, β and γ-coefficients [18], and established that the phonon excitations at these points are classified with one-valued projective representations of the projective class K_5 and the electronic excitations – with two-valued projective representations of the projective class K_4. The

Table 2. **Matrices of irreducible projective representation of projective class K_5 for standard factor-system $\omega'_{(5)}(r_2, r_1)$ of the group 6/mmm (D_{6h}).**

Represent.	e	c_3	c_3^2	$(u_2)_1$	$(u_2)_2$	$(u_2)_3$	c_2	c_6^5	c_6	$(u_2')_1$	$(u_2')_2$	$(u_2')_3$
$P_1^{(5)}$	$\begin{pmatrix}1&0\\0&1\end{pmatrix}$	$\begin{pmatrix}1&0\\0&1\end{pmatrix}$	$\begin{pmatrix}1&0\\0&1\end{pmatrix}$	$\begin{pmatrix}0&1\\1&0\end{pmatrix}$	$\begin{pmatrix}0&1\\1&0\end{pmatrix}$	$\begin{pmatrix}0&1\\1&0\end{pmatrix}$	$\begin{pmatrix}1&0\\0&-1\end{pmatrix}$	$\begin{pmatrix}1&0\\0&-1\end{pmatrix}$	$\begin{pmatrix}1&0\\0&-1\end{pmatrix}$	$\begin{pmatrix}0&1\\-1&0\end{pmatrix}$	$\begin{pmatrix}0&1\\-1&0\end{pmatrix}$	$\begin{pmatrix}0&1\\-1&0\end{pmatrix}$
Represent.	i	ic_3	ic_3^2	$(\sigma_d)_1$	$(\sigma_d)_2$	$(\sigma_d)_3$	σ_h	ic_6^5	ic_6	$(\sigma_d')_1$	$(\sigma_d')_2$	$(\sigma_d')_3$
$P_1^{(5)}$	$\begin{pmatrix}0&1\\1&0\end{pmatrix}$	$\begin{pmatrix}0&1\\1&0\end{pmatrix}$	$\begin{pmatrix}0&1\\1&0\end{pmatrix}$	$\begin{pmatrix}1&0\\0&1\end{pmatrix}$	$\begin{pmatrix}1&0\\0&1\end{pmatrix}$	$\begin{pmatrix}1&0\\0&1\end{pmatrix}$	$\begin{pmatrix}0&-1\\1&0\end{pmatrix}$	$\begin{pmatrix}0&-1\\1&0\end{pmatrix}$	$\begin{pmatrix}0&-1\\1&0\end{pmatrix}$	$\begin{pmatrix}-1&0\\0&1\end{pmatrix}$	$\begin{pmatrix}-1&0\\0&1\end{pmatrix}$	$\begin{pmatrix}-1&0\\0&1\end{pmatrix}$

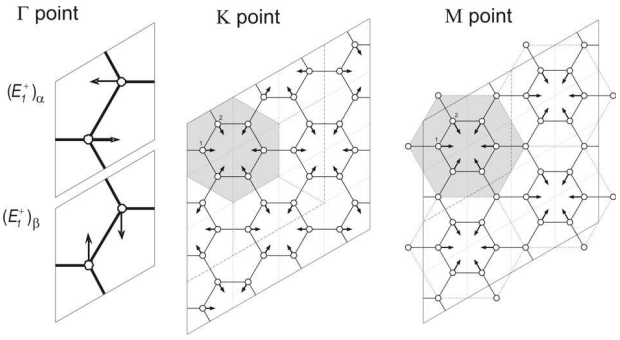

Fig. 6. Forms of stationary elastic waves for one-layer graphene at Γ, K, and M points of its Brillouin zone

projective irreducible representations of these classes are presented in Table 1 [12]. The degenerated representations of the projective classes K_5 and K_4 for A-points are appeared as a result of the joints of complex conjugated representations. All projective representations at Γ-points and representations A_1, A_2, A_3, and A_6 belong to the case a_1 [12], and representations A_4 and A_5 belong to the case b_1. The representations at Δ-points lying on Γ-A line belong to a_1 case. So, only the irreducible representations A_4 and A_5 are joint.

Figure 5 shows the compatibility relations for irreducible projective representations of the $P6_3/mmc(D_{6h}^4)$ and CSG D_{6h}–1 space symmetry groups along Γ–Δ–A Brillouin zone lines. We can see that all dispersion branches at A-points for bulk graphite crystals and for SWCNTs joint pairwise.

Using the standard method of application of the projection operator of irreducible representations, we firstly analytically calculated the forms of normal

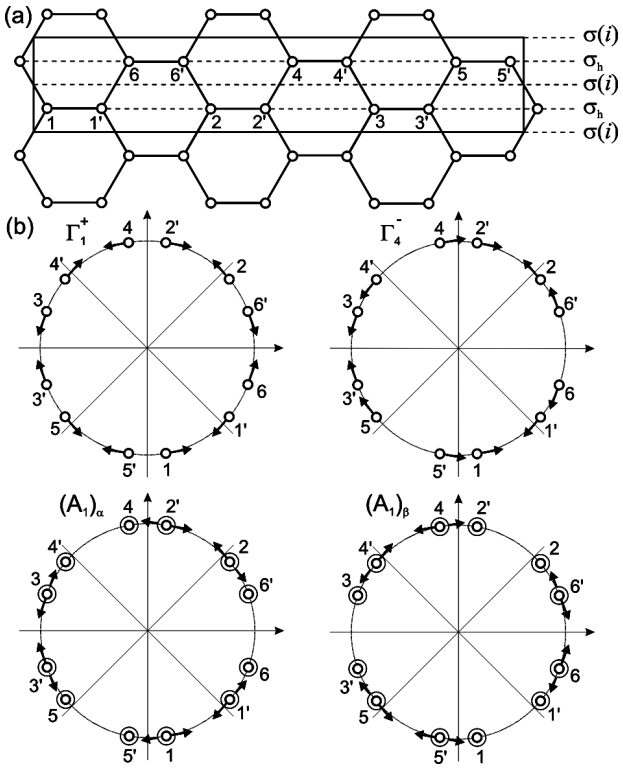

Fig. 7. Evolvent of armchair (3, 3) carbon nanotube fragment (a) and forms of normal vibrations at Γ-point (Γ_1^+, Γ_4^-) and A-point ($(A_1)_\alpha, (A_1)_\beta$) of the nanotube Brillouin zone

vibrations of SWCNTs at Γ and A points of their Brillouin zones; one- and two-layer graphenes at Γ, K, and M points of their Brillouin zones, and bulk graphite at Γ, K, and M points. We used the matrices of irreducible projective representation of the projective class K_5 for the analytic calculation of

forms of normal vibrations of SWCNTs at A points for symetry A_1, which are presented in Table 2.

The forms of vibrations corresponding to stationary elastic waves of one-layer graphene at Γ, K, and M points of its Brillouin zone are presented in Fig. 6 and, for SWCNTs at A points of their Brillouin zones with symmetry A_1, are presented in Fig. 7. Stationary elastic waves at $\mathbf{k} \neq 0$ points are obtained, by summing the displacements of atoms through all rays of the wave vector star of the corresponding point. The calculated forms of normal vibrations are useful for the determination of dynamic force matrices of carbon structures under investigation and can be used for numerical calculations of their dynamics.

1. K.S. Novoselov, A.K. Geim, S.V. Morozov, D. Jiang, Y. Zhang, S.V. Dubonos, I.V. Grigorieva, and A.A. Firsov, Science **306**, 666 (2004).
2. L.M. Malard, M.A. Pimenta, G. Dresselhaus, and M.S. Dresselhaus, Phys. Rep. **473**, 51 (2009).
3. B. Partoens and F.M. Peeters, Phys. Rev. B **74**, 075404 (2006).
4. A.C. Ferrari and J. Robertson, Phys. Rev. B **61**, 14095 (2000).
5. M.A. Pimenta, G. Dresselhaus, M.S. Dresselhaus, L.G. Cancado, A. Jorio, and R. Saito Phys. Chem. Chem. Phys. **9**, 1276 (2007).
6. M.S. Dresselhaus, G. Dresselhaus, A. Jorio, A.G. Souza Filho, M.A. Pimenta, and R. Saito, Acc. Chem. Res. **35**, 1070 (2002).
7. P. Blakea, E.W. Hill, A.H. Castro Neto, K.S. Novoselov, D. Jiang, R. Yang, T.J. Booth, and A.K. Geim, Appl. Phys. Lett. **91**, 063124 (2007).
8. A.C. Ferrari, J.C. Mayer, V. Scardaci, C. Casiraghi, M. Lazzeri, F. Mauri, S. Piscanec, D. Jiang, K.S. Novoselov, S. Roth, and A.K. Geim, Appl. Phys. Lett. **97**, 187401 (2006).
9. T. Michel, M. Paillet, A. Zahab, D. Nakabayashi, V. Jourdain, R. Parret, and J.-L. Sauvajol, Adv. Nat. Sci.: Nanosci. Nanotechnol. **1**, 045007 (2010).
10. L.M. Malard, M.H.D. Guimarães, D.L. Mafra, M.S.C. Mazzoni, and A. Jorio, Phys. Rev. B **79**, 125426 (2009).
11. M.C. Schabel, and J.L. Martins, Phys. Rev. B **46**, 7185 (1992).
12. G.L. Bir and G.E. Pikus *Symmetry and Strain-Induced Effects in Semiconductors* (Wiley, New York, 1974).
13. L.G. Cancado, A. reina, J. Kong, and M.S. Dresselhaus, Phys. Rev. Lett. **77**, 245408 (2008).
14. M. Damnjanović, T. Vuković, I. Milošević, and B. Nikolić, Acta Crystallogr. A **57**, 304 (2001).
15. O.E. Alon, Phys. Rev. B **63**, 201403 (2001).
16. E.A. Wood, Bell System Techn. J. **43**, 541 (1964).
17. T. Hahn, *International Tables for Crystallography* (Reidel, Dordrecht, 1987), Vol. A, Space-group symmetry.
18. V.O. Gubanov, L.O. Komarova, M.M. Biliy, and S.V. Kovrygin, Nanosyst., Nanomater., Nanotechn. **5**, 307 (2007).

Received 15.06.15

В.В. Стрельчук, А.С. Ніколенко, Ю.Ю. Стубров, О.Є. Беляєв, В.О. Губанов, М.М. Білий, Л.А. Булавін

ЕНЕРГЕТИЧНІ СПЕКТРИ ФОНОНІВ ТА СТАЦІОНАРНІ ПРУЖНІ ХВИЛІ В ОДНОСТІННИХ ВУГЛЕЦЕВИХ НАНОТРУБКАХ ТА КРИСТАЛАХ ГРАФІТУ

Р е з ю м е

Проаналізовано спектри комбінаційного розсіяння світла (мікро-КРС) одностінних вуглецевих нанотрубок, кристалічного графіту, одно- та двошарового графенів. Встановлено структури давидівських мультиплетів в енергетичних спектрах електронних станів одно- і двошарового графенів та кристалічного графіту. Показано, що енергетичний спектр коливних та електронних станів вуглецевих нанотрубок і кристалічного графіту можна описати дисперсійними кривими, які попарно об'єднуються в точках А зон Бріллюена цих структур. Аналітично розраховано форми коливань у стаціонарних пружних хвилях для одностінних нанотрубок в точках Γ і А їх зон Бріллюена та для одно- та двошарового графенів і кристалічного графіту в точках Γ, K і M відповідних їм зон Бріллюена.